

## Article

# Reliability Evaluation of Standalone Microgrid Based on Sequential Monte Carlo Simulation Method

Zhipeng Weng, Jinghua Zhou \* and Zhengdong Zhan

Inverter Technology Engineering Research Center of Beijing, North China University of Technology, Beijing 100144, China

\* Correspondence: zjh@ncut.edu.cn

**Abstract:** In order to analyze the influence of uncertainty and an operation strategy on the reliability of a standalone microgrid, a reliability evaluation method based on a sequential Monte Carlo (SMC) simulation was developed. Here, the duty cycles of a microturbine (MT), the stochastic performance of photovoltaics (PV), and wind turbine generators (WTG) were considered. Moreover, the time-varying load with random fluctuation was modeled. In this method, the available capacity of an energy storage system (ESS) was also comprehensively considered by the SMC simulation. Then, the reliability evaluation framework was established from the perspectives of probability, frequency, and duration, and reliability evaluation algorithms under different operation strategies were formulated. Lastly, the influence of WTG and PV penetration and equipment capacity on the reliability was evaluated in the test system. The results showed that the complementary characteristics of wind and solar and the enhancement of the equipment capacity can both improve the reliability; but, with the increase in the penetration rate of WTG and PV, more ESS capacity is needed to cope with the randomness of WTG and PV. In addition, load shedding minimization strategies can minimize the probability and the number of reductions and achieve optimal reliability, which can provide a reference for the formulation of microgrid operation strategies.



**Citation:** Weng, Z.; Zhou, J.; Zhan, Z. Reliability Evaluation of Standalone Microgrid Based on Sequential Monte Carlo Simulation Method. *Energies* **2022**, *15*, 6706. <https://doi.org/10.3390/en15186706>

Academic Editors: Josue Campos do Prado and Luciane Neves Canha

Received: 25 July 2022

Accepted: 31 August 2022

Published: 14 September 2022

**Publisher's Note:** MDPI stays neutral with regard to jurisdictional claims in published maps and institutional affiliations.



**Copyright:** © 2022 by the authors. Licensee MDPI, Basel, Switzerland. This article is an open access article distributed under the terms and conditions of the Creative Commons Attribution (CC BY) license (<https://creativecommons.org/licenses/by/4.0/>).

**Keywords:** microgrid; sequential Monte Carlo simulation; energy storage system; reliability evaluation; load shedding

## 1. Introduction

At present, China is stepping up the construction of a new power system with new energy as the main body and is committed to the realization of the “double carbon” goal [1]. As an important technical system for the large-scale access of renewable energy, the microgrid is used to ensure a reliable power supply to loads in home communities, industrial parks, isolated islands, and remote areas that are difficult to reach for power grid construction.

Compared with the conventional grid, the power supply reliability and evaluation method of the standalone microgrid have the following characteristics. (1) The power supply reliability of the standalone microgrid is more susceptible to the intermittent output from internal distributed energy sources (such as photovoltaics (PV) and wind turbine generators (WTG)) and diversified energy management strategies (such as load control, energy storage scheduling). (2) Due to the lack of power support from the main grid, the real-time power balance relationship of the standalone microgrid is more complex, which puts forward higher requirements for reliability evaluation [2]. (3) It is difficult for traditional reliability evaluation methods to accurately reflect the output state and component timing characteristics of a standalone microgrid, and a reliability evaluation method based on islanding characteristics is urgently needed.

To solve these problems, a great deal of literature was studied. From the perspective of energy storage system (ESS) operation, the literature [3] discusses the impact of load

shedding strategies on reliability, such as smoothing the random output of distributed generation (DG), limiting DG penetration beyond the limit, and utilizing the maximum charge and discharge characteristics of ESS. The results showed that ESS can reduce the probability of load shedding, if required. According to the load importance level, some of the literature [4,5] uses the block method to determine the load shedding order, which makes the load point reliability show a large difference. It was shown that paying attention to load location and importance is necessary for load point reliability evaluation. S. Bahramirad et al. [6] took the loss of load expectation (LOLE) as a reliability constraint to seek the economical optimum in ESS capacity planning. Its power dispatch and load reduction strategy can only slightly improve reliability on the basis of keeping a power balance and a minimum operating cost and cannot evaluate the highest reliability level that the microgrid can achieve. One item of the literature [7], taking the minimum load shedding as the dispatching objective, provides a unified evaluation benchmark for the comparison and selection of the reliability level of the microgrid under different capacity configuration schemes, which has reference significance for the research of this paper.

From the above discussion, most researchers only treat the reliability index as a constraint in capacity planning or operation strategy formulation. However, in fact, reliability is very important for the microgrid, especially for a standalone microgrid, which deserves in-depth study. Moreover, the uncertainty of the standalone microgrid is very complex, and the supply and demand sides interact frequently. Therefore, the more comprehensive the reliability index is, the more accurately the reliability of the standalone microgrid can be reflected. The contributions of this paper are as follows:

- (1) Uncertainty characteristics of the microturbine (MT), WTG, PV, ESS, and load were studied by using the sequential Monte Carlo (SMC) simulation method.
- (2) Reliability evaluation algorithms under two microgrid operation strategies were formulated, and the effects of the WTG, PV penetration rate, and equipment capacity changes on microgrid reliability were evaluated from the perspectives of probability, frequency, and duration.

The rest of the paper is arranged as follows. We demonstrate the microgrid system model in Section 2 and the reliability evaluation in Section 3, including establishing the indicators' evaluation framework, formulating the load shedding strategy and the evaluation algorithm based on SMC. In Section 4, the reliability evaluation is analyzed, followed by the conclusions of the paper in Section 5.

## 2. Microgrid System Model

### 2.1. Microgrid System Structure

In this work, the main feeder F4 of the improved RBTS BUS6 system was used as the test system, and the microgrid was connected to the branch line 25, as shown in Figure 1. The improved RBTS BUS6 system had a total of 23 loads, and some branches were equipped with intelligent switches, which could effectively cut off the load current. The microgrid system studied in this work was composed of an MT, WTG, PV, ESS, and load, as shown in Figure 1, where LP represents the load point (LP) on the system, and numbers 1 to 30 represents the branch line 1 to 30.

As we can see in Figure 1, due to the lack of energy support from the upper-level grid, it was necessary to keep a real-time power balance between the supply and demand sides:

$$P_L(h) = P_{MT}(h) + P_{PV}(h) + P_{WTG}(h) + P_{ESS}(h) \quad (1)$$

where  $P_L(h)$  is the total load power,  $P_{MT}(h)$  is the MT power output,  $P_{PV}(h)$  is the PV power output,  $P_{WTG}(h)$  is the WTG power output, and  $P_{ESS}(h)$  is the ESS power output.

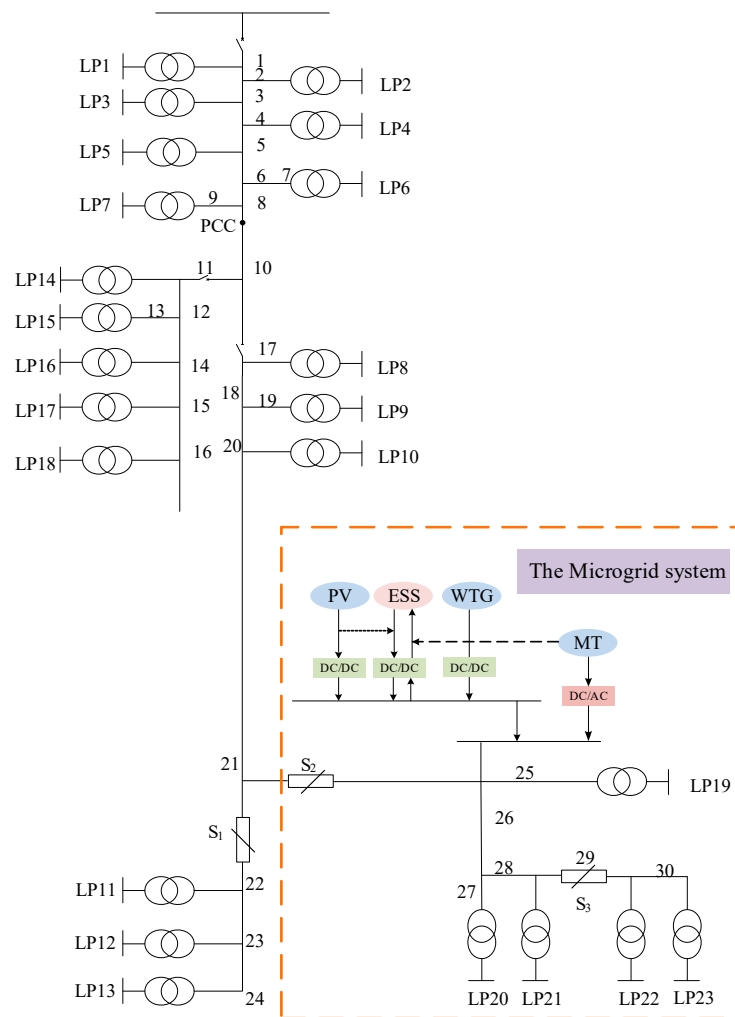


Figure 1. The structure of the microgrid system.

2.2. Sequential Model of Component Life Process

From the perspective of time, the life process of a component is generally composed of a series of fault free working state sequences,  $T_{TTF,i}$  and faulty working state sequence,  $T_{TTR,i}$  [8], as shown in Equations (2) and (3).

$$T_{TTF,i} = (-\lambda_i)^{-1} \ln u_i \tag{2}$$

$$T_{TTR,i} = (-\mu_i)^{-1} \ln \zeta_i \tag{3}$$

where  $\lambda_i$  and  $\mu_i$  are the failure and repair rates of component  $i$ , respectively. The  $u_i$  and  $\zeta_i$  are random variables that obey the uniform distributions between 0 and 1.

2.3. MT Power Output Model

The MT is a common and important part of the microgrid system, which can be used as a standing power supply or to provide emergency power support. Therefore, the MT output model considering fault characteristics was established, as shown in Equations (4) and (5).

$$0 \leq P_{MT}(h) \leq P_{MT}^{max}(h)F_{MT}(h) \tag{4}$$

$$F_{MT}(h) = \begin{cases} 1, & \text{when } h \in T_{TTF,i}^{MT} \\ 0, & \text{when } h \in T_{TTR,i}^{MT} \end{cases} \tag{5}$$

Where  $P_{MT}^{max}(h)$  is the MT maximum power output at the  $h$ -th moment,  $F_{MT}(h)$  is the working state function of the MT, and  $T_{TTF,i}^{MT}$  and  $T_{TTR,i}^{MT}$  are the fault free working state sequence and the faulty working state sequence of the MT, respectively.

#### 2.4. WTG Power Output Model

The maximum power output per hour of the WTG,  $P_{WTG}^{max}(h)$ , is a nonlinear function of wind speed [9], as shown in Equation (6). When the wind speed  $V$  is between the cut-in wind speed  $V_{ci}$  and the rated wind speed  $V_r$ ,  $P_{WTG}^{max}(h)$  varies linearly with  $V$ . When  $V$  is between the  $V_r$  and the cut-out wind speed  $V_{co}$ ,  $P_{WTG}^{max}(h)$  equals the rated power  $P_r$ . Otherwise,  $P_{WTG}^{max}(h)$  is 0. Therefore, by comparing  $V$  with  $V_{ci}$ ,  $V_{co}$  and  $V_r$ ,  $P_{WTG}^{max}(h)$  is generated hour by hour with stochastic performance. In this paper,  $V_{ci}$ ,  $V_{co}$  and  $V_r$  are 3 m/s, 20 m/s, and 10 m/s, respectively. The  $V_{ci}$ ,  $V_{co}$  and  $V_r$  are also determined by the annual wind speed, wind power generation, and WTG equipment model in the area. Then, the WTG power output,  $P_{WTG}(h)$ , can be described by Equations (7) and (8).

$$P_{WTG}^{max}(h) = \begin{cases} P_r \frac{V-V_{ci}}{V_r-V_{ci}}, & V_{ci} \leq V \leq V_r \\ P_r, & V_r \leq V \leq V_{co} \\ 0, & other \end{cases} \quad (6)$$

and

$$0 \leq P_{WTG}(h) \leq P_{WTG}^{max}(h)F_{WTG}(h) \quad (7)$$

$$F_{WTG}(h) = \begin{cases} 1, & \text{when } h \in T_{TTF,i}^{WTG} \\ 0, & \text{when } h \in T_{TTR,i}^{WTG} \end{cases} \quad (8)$$

where  $F_{WTG}(h)$  is the working state function of the WTG, and  $T_{TTF,i}^{WTG}$  and  $T_{TTR,i}^{WTG}$  are the fault free working state sequence and the faulty working state sequence of the WTG, respectively.

Since the uncertainty characteristics of a microgrid are very complex, we extracted its typical characteristics when building the WTG model. On the premise that the relationship between the WTG output and wind speed can be reflected, the authors idealized the WTG model on a unified time scale. However, it should also be noted that the possible value and probability distribution of the wind speed at different scales should also be fully considered. By establishing probability density functions at different wind speed scales, the WTG model can be more perfect [9].

It can be seen from Equation (8) that the WTG power output is not only related to the maximum output power of the WTG but also determined by the working state of the WTG. The above equations constitute the WTG power output model, which reflects the randomness attribute and timing life attribute of the WTG output.

#### 2.5. PV Power Output Model

The intermittency and randomness are the dominant features of a PV power output, which will affect the reliability of the microgrid. The PV power output model with a beta probability density function during the daytime is shown in Equations (9) and (10) [10].

$$P_{PV}(h) = \begin{cases} 0, & \text{when } h \in [0, T_{sun}^{rise}) \\ P_{PV}^{avail}(h), & \text{when } h \in [T_{sun}^{rise}, T_{sun}^{down}] \\ 0, & \text{when } h \in (T_{sun}^{down}, 24) \end{cases} \quad (9)$$

and

$$f(P_{PV}^{avail}(h)) = \frac{\Gamma(\alpha + \beta)}{\Gamma(\alpha)\Gamma(\beta)} \left( \frac{P_{PV}^{avail}(h)}{P_{PV}^{max}(h)} \right)^{\alpha-1} \left( 1 - \frac{P_{PV}^{avail}(h)}{P_{PV}^{max}(h)} \right)^{\beta-1} \quad (10)$$

where  $P_{PV}^{avail}(h)$  is the PV power output during the illumination period,  $T_{sun}^{rise}$  is the sunrise time and equals 6 h,  $T_{sun}^{down}$  the sunset time and equals 18 h,  $f(P_{PV}^{avail}(h))$  is the distribution

function of  $P_{PV}^{avail}(h)$ ,  $\Gamma$  is the Gamma function, and  $\alpha$  and  $\beta$  are the shape parameters of the beta distribution, which are set to 2 and 0.8, respectively.

In mathematics, the probability density function of a continuous random variable is a function that describes the probability that the output value of the random variable will be near a certain value point. Combined with the content of the paper,  $f(P_{PV}^{avail}(h))$  is a continuous random variable and a certain value point corresponds to density while probability corresponds to probability. The  $f(P_{PV}^{avail}(h))$  describes the probability of  $P_{PV}^{avail}(h)$  in the vicinity of a certain value. In other words,  $f(P_{PV}^{avail}(h))$  is a functional form that describes the possibility of  $P_{PV}^{avail}(h)$  being around a certain output value.

Combined with Equations (9) and (10), the PV power output  $P_{PV}(h)$  considering the fault characteristics is obtained, as shown in Equations (11) and (12).

$$0 \leq P_{PV}(h) \leq P_{PV}^{avail}(h)F_{PV}(h) \quad (11)$$

$$F_{PV}(h) = \begin{cases} 1, & \text{when } h \in T_{TTF,i}^{PV} \\ 0, & \text{when } h \in T_{TTR,i}^{PV} \end{cases} \quad (12)$$

where  $F_{PV}(h)$  is the working state function of the PV, and  $T_{TTF,i}^{PV}$  and  $T_{TTR,i}^{PV}$  are the fault free working state sequence and the faulty working state sequence of the PV, respectively.

Equation (12) describes the working state function of PV. In short, it is to judge the working state of PV by 0 and 1. In the manuscript, 1 means the PV is in a fault free state, which means the PV is in normal operation, and 0 means the PV is in a fault state. In general,  $f(P_{PV}^{avail}(h))$  and  $F_{PV}(h)$  are both functions, but they describe different objects. The  $f(P_{PV}^{avail}(h))$  describes the probability density of  $P_{PV}^{avail}(h)$ , while  $F_{PV}(h)$  describes the state of the PV, normal or faulty.

## 2.6. ESS Model

ESS plays an important role in smoothing the fluctuation of renewable energy and maintaining the stability of a power supply. For lead-acid batteries, the ESS model based on state of charge (SOC) is established [11].

$$S_{SOC}(h) = (1 - \delta)S_{SOC}(h - 1) + \frac{P_{ch}(h)\Delta t\eta_{ch}}{E_{ESS}^{max}}F_{ch}(h) - \frac{P_{dch}(h)\Delta t}{E_{ESS}^{max}\eta_{dch}}F_{dch}(h) \quad (13)$$

and

$$F_{ch}(h) = \begin{cases} 1, & \text{when ESS is charging state} \\ 0, & \text{when ESS is discharging state} \end{cases} \quad (14)$$

$$F_{ch}(h) + F_{dch}(h) = 1 \quad (15)$$

$$S_{SOC}^{min} \leq S_{SOC}(h) \leq S_{SOC}^{max} \quad (16)$$

$$S_{SOC}(h) = E_{ESS}(h) / E_{ESS}^{max} \quad (17)$$

where  $S_{SOC}(h)$  is the SOC of ESS at the  $h$ -th moment and initialized as 0.5,  $\delta$  is the ESS self-discharging rate and initialized as 0.001, and  $P_{ch}(h)$  and  $P_{dch}(h)$  are the charging and discharging powers, respectively. The  $\eta_{ch}$  and  $\eta_{dch}$  are the charging and discharging efficiencies, respectively, which are both set to 0.9,  $\Delta t$  is the simulation step and assumed as 1 h,  $E_{ESS}^{max}$  is the upper limit of ESS capacity, and  $F_{ch}(h)$  and  $F_{dch}(h)$  are the state functions of charging and discharging, respectively.  $S_{SOC}^{max}$  is the upper limit of the SOC and is set to 0.9, and  $S_{SOC}^{min}$  is the lower limit of the SOC and is set to 0.2.

## 2.7. Load Comprehensive Model

The fluctuation of load is greatly affected by hourly time varying and randomness, especially in different time scales [12]. Therefore, Equations (18)–(20) can be used to reflect its fluctuation.

$$P_L(h) = P_L^T(h) + P_L^R(h) \quad (18)$$

and

$$P_L^T(h) = P_y P_{y-m} P_{m-d} P_{d-h} \tag{19}$$

$$f(P_L^R(h)) = \frac{1}{\sqrt{2\pi}\sigma_L} \exp\left(-\frac{(P_L^R(h) - \mu_L)^2}{2\sigma_L^2}\right) \tag{20}$$

where  $P_L^T(h)$  and  $P_L^R(h)$  are the hourly time-varying component and randomness component, respectively,  $P_y$  is the annual peak load,  $P_{y-m}$  is the percentage of the monthly peak load to the annual peak load,  $P_{m-d}$  is the percentage of the daily peak load to the monthly peak load,  $P_{d-h}$  is the percentage of hourly peak load to the daily load, and  $f(P_L^R(h))$  is the density function of load randomness, and its expectation and standard deviation are  $\mu_L$  and  $\sigma_L$ , respectively.

In the process of modeling the microgrid system, this work considered the fault and timing characteristics of each component, the uncertainty of WTG and PV power output, the power characteristics of ESS, and the hourly time varying and randomness of the load. The change curves of WTG and PV power, load, SOC, and ESS power within 1 week (5358 h~5526 h), from 6 h on 10 August to 6 h on 17 August in the first year of simulation, are shown in Figures 2 and 3.

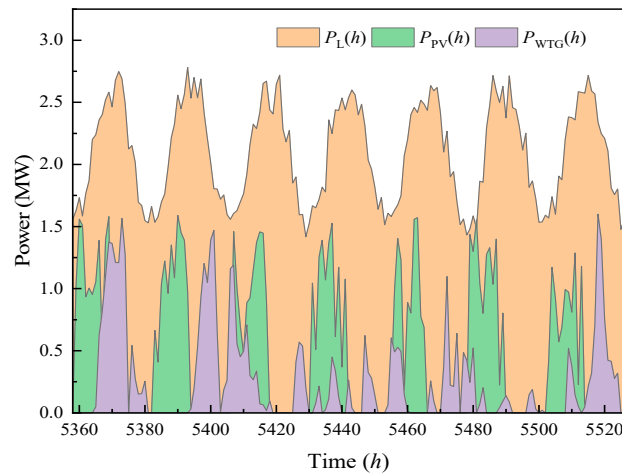


**Figure 2.** Change curves of wind turbine generators (WTG), photovoltaics (PV), and load power within 1 week.

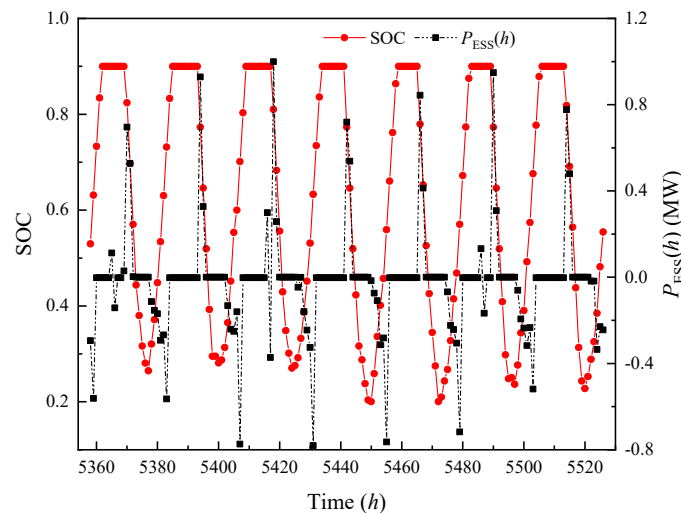


**Figure 3.** Change curves of energy storage system (ESS) power and state of charge (SOC) within 1 week.

### 3. Establishment of Reliability Evaluation Framework and Formulation of Load Shedding Strategies

#### 3.1. Establishment of Reliability Evaluation Framework

Numerous reliability indicators and algorithms have been proposed in many items of literature. These indicators are weighted and integrated by factors such as technology, economy, environment, or comprehensive benefits. The literature [13] used scenario generation and reduction technology, which generates multiple scenarios for power supply capability evaluation from the perspective of probability; the selection of reliability indicators also focuses on the probability dimension. However, the non-sequential Monte Carlo (NSMC) simulation method adopted in [14] combines a variety of sampling methods, focusing on the accuracy and computational efficiency of reliability evaluation. Based on the established microgrid model, the SMC algorithm carried out reliability evaluation. Compared with the scenario analysis method [13] and the NSMC simulation method [14], the SMC can obtain two types of reliability data. One is probability indicators, which includes the loss of load probability (LOLP) and the average service availability index (ASAI). The other is frequency and duration indicators, which include the system average interruption frequency index (SAIFI) and the system average interruption duration index (SAIDI).

Firstly, two types of reliability data can comprehensively reflect the reliability of the microgrid, which can be more suitable for describing different types of load demands. For example, LOLP and ASAI can reflect the probability of a power shortage and the available power for users from the perspective of probability. SAIFI and SAIDI can describe the number and the duration of the outage.

Secondly, two types of data can fully evaluate the adequacy of the microgrid in terms of power and energy, which are more suitable for the reliability evaluation of the microgrid equipped with intermittent power sources such as PV and WTG and power/energy buffer links such as ESS. In addition, it is also convenient to extend the indicators' system to the evaluation system of other dimensions such as economic evaluation, comprehensive operation benefit evaluation, etc. These two types of indicators are widely used in the reliability evaluation of conventional power systems and can effectively support the reliability evaluation of microgrids.

Considering the above factors, a reliability evaluation framework including LOLP, ASAI, SAIDI, and SAIFI was established [15–18].

##### 3.1.1. Reflecting the Reliability of Microgrid System from the Probabilistic Level

- (1) LOLP can represent the probability that the system cannot meet the load demand within the total simulation time, as shown in Equations (21) and (22).

$$R_{\text{LOLP}} = \frac{1}{H} \sum_{h=1}^H F_{\text{LOLP}}(h) \quad (21)$$

and

$$F_{\text{LOLP}}(h) = \begin{cases} 0, & P_L(h) \leq P_{\text{PV}}(h) + P_{\text{MT}}(h) + P_{\text{WTG}}(h) + P_{\text{ESS}}(h) \\ 1, & P_L(h) > P_{\text{PV}}(h) + P_{\text{MT}}(h) + P_{\text{WTG}}(h) + P_{\text{ESS}}(h) \end{cases} \quad (22)$$

where  $F_{\text{LOLP}}(h)$  is the state function of LOLP and  $H$  is the total simulation time.

- (2) ASAI can represent the probability that the system does not have a power outage within the total simulation time, as shown in Equation (23).

$$R_{\text{ASAI}} = \frac{H \sum_i^{N_{\text{LP}}} N_i - \sum_i^{N_{\text{LP}}} U_i N_i}{H \sum_i^{N_{\text{LP}}} N_i} \quad (23)$$

where  $U_i$  and  $N_i$  are the annual outage time and the number of users of load point  $i$ , respectively, and  $N_{\text{LP}}$  is the total number of load points.

### 3.1.2. Reflecting the Reliability of Microgrid System from the Frequency and Duration level

- (1) SAIDI can represent the average power outage hours of the system within the total simulation time, as shown in Equation (24).

$$R_{SAIDI} = \frac{\sum_i^{N_{LP}} U_i N_i}{\sum_i^{N_{LP}} N_i} \quad (24)$$

- (2) SAIFI can reflect the average power failure frequency of the system within the total simulation time, as shown in Equation (25).

$$R_{SAIFI} = \frac{\sum_i^{N_{LP}} \lambda_i N_i}{\sum_i^{N_{LP}} N_i} \quad (25)$$

where  $\lambda_i$  is the annual power failure frequency of  $i$ -th load point.

### 3.2. Formulation of Load Shedding Strategies

Load shedding strategies have a significant impact on the reliability level of microgrids. Therefore, considering the power balance of the microgrid system, the following strategies were established and compared by simulation. For a standalone microgrid, the reliability of the system is more susceptible to the interference of distributed energy output characteristics, component reliability, ESS operation mode, and load sequences fluctuation. Due to the lack of energy support from the upper-level grid, a real-time power balance between supply and demand needs to be maintained. Therefore, the load shedding strategy is particularly important for a standalone microgrid. As shown below, two load shedding strategies under different operating objectives were proposed.

#### 3.2.1. Strategy A: Aim to Load Shedding Minimization

Scenario 1: If the combined power (WTG and PV) is greater than the load demand, then the excess combined power is absorbed by the ESS and there is no load shedding at this time.

Scenario 2: If the combined power (WTG, PV, and MT) is greater than the load demand, then the excess combined power is absorbed by the ESS and there is no load shedding at this time.

Scenario 3: If the combined power (WTG, PV, MT, and ESS) is greater than the load demand, there is no load shedding at this time. (In this scenario, WTG, PV, and MT are at maximum power state and ESS is in discharge or maximum discharge state.)

Scenario 4: If the combined power (WTG, PV, MT, and ESS) is less than the load demand, the microgrid power is in a state of insufficient power and needs load shedding at this time. (In this scenario, WTG, PV, and MT are at maximum power state and ESS is in maximum discharge state.)

#### 3.2.2. Strategy B: Aim to Limit the Penetration of Renewable Energy

In this work, the combined power of WTG and PV did not exceed 30% of the load demand.

Scenario 1: If the combined power (WTG and PV) is less than 30% of the load demand, then the load shortfall power is supplied by the MT, the redundant MT power is used to charge the ESS, and there is no load shedding at this time.

Scenario 2: If the combined power (WTG and PV) is less than 30% of the load demand, ESS is discharged and the MT starts to work. If the load demand cannot be met after the MT output, then load will be reduced.

Scenario 3: If the combined power (WTG and PV) is greater than 30% of the load demand, the redundant power is used to charge the ESS and the MT starts to work. If the MT power meets the load shortfall power, there is no load shedding at this time.

Scenario 4: If the combined power (WTG and PV) is greater than 30% of the load demand, the redundant power is used to charge the ESS and the MT starts to work. If the maximum power of the MT still cannot meet the load shortfall power, then the load will be reduced at this time.

Firstly, the definition of a renewable energy penetration rate should be given: It refers to the ratio of the total electricity provided by renewable energy in the whole year to the total electricity consumption of the load in the power supply area in the whole year. That is, what percentage of the load demand can be met by the electricity generated by renewable energy. Due to the advantages of environmental friendliness and non-polluting emissions, renewable energy is widely used all over the world. As the penetration rate of renewable energy increases year by year, the randomness, volatility, and intermittent characteristics of renewable energy have an increasing impact on the safe and stable operation of the microgrid system. When the penetration rate of renewable energy exceeds 30%, the renewable energy system is called a high-proportion renewable energy system in China. Different from general renewable energy systems, the connection of a high proportion of renewable energy brings strong uncertainty to the system, which makes the interaction between the power supply and load demand more frequent, which brings great challenges to reliability evaluation and system planning. Therefore, it is necessary to qualitatively study the impact of renewable energy penetration on the reliability of microgrids and then provide a reference for quantitative evaluation. For the above purpose, the authors set the initial value of penetration to 30%. At the same time, it should be noted that the initial value can be adjusted according to the experimental needs, which are also reflected in the experiments in Section 4.3.

The basic principle of strategy B is that PV, WTG, and ESS give power to a part of the load first, that is, 30% of the load demand, and MT not only supplies power to other loads but also serves as a backup power source for PV, WTG, and ESS. In strategy B, we made the PV and WTG output stable and controllable by rationally utilizing the charge and discharge characteristics of the ESS. However, this stability and control also limits the charging and discharging of ESS. For example, when the load needs a power supply of 100 kW, the PV and WTG need to supply 30 kW according to the strategy B. When the PV and WTG power output exceeds 30 kW, the ESS begins to absorb the excess power for use at the next moment. At this point, if the MT power output is greater than 70 kW, the excess power is used to charge the ESS, but when the MT power output is less than 70 kW, the load is reduced, even if the residual capacity of ESS is still enough. Since the ESS function is only used for stable and controllable PV and WTG power output, the above situation increases the probability and quantity of load shedding, which is not conducive to the reliability under strategy B. This conclusion is also verified in Section 4.1 to Section 4.3 of the paper. However, in practical applications, it is not easy to realize the coordinated output between distributed energy resources and ESS. In fact, some converter interfaces, collectors, communication equipment, etc. are needed to assist in the realization of simulation program functions. In this study, only the critical facilities, such as PV, WTG, ESS, etc., were comprehensively taken into consideration. Furthermore, we assumed that converters and other complementary equipment contributed marginally to the system reliability. In this way, the varying characteristics of reliability with different capacities of PV, WTG, and ESS could be observed.

Comparing the above strategies, it can be seen that strategy A tracked the load demand in real time, planned the output of MT, WTG, PV, and ESS, and took the principle of giving priority to renewable energy generation and consumption to achieve load shedding minimization. Strategy B reduced the amount of ESS stabilization while maintaining the system power balance and reducing the impact of WTG and PV uncertainty on the microgrid system by limiting the penetration of renewable energy.

### 3.3. Reliability Evaluation Algorithm Based on SMC

By sampling the state durations of all components, the traditional SMC algorithm could obtain the sequential state of the system and perform a reliability analysis. Compared to the conventional grid, the existence of distributed energy and ESS in the standalone microgrid made the output of the microgrid random and sequential, and its fault state directly affected the reliability of the microgrid. Therefore, the reliability evaluation algorithm based on the SMC simulation was proposed, taking into account the failure states of the MT, WTG, PV, ESS, and other components. The SMC method can obtain abundant reliability data and generate three types of reliability indicators: probability, frequency, and duration. During the total simulation time, the duration of the states of all components was randomly sampled many times and the state alternation process of operation–repair–operation–repair of each component in the  $n$ -th year was obtained. The system state sequences with chronological order were obtained by combining the state transition processes of the components. The flow chart of the reliability evaluation algorithm under the two strategies is given, as shown in Figure 4.

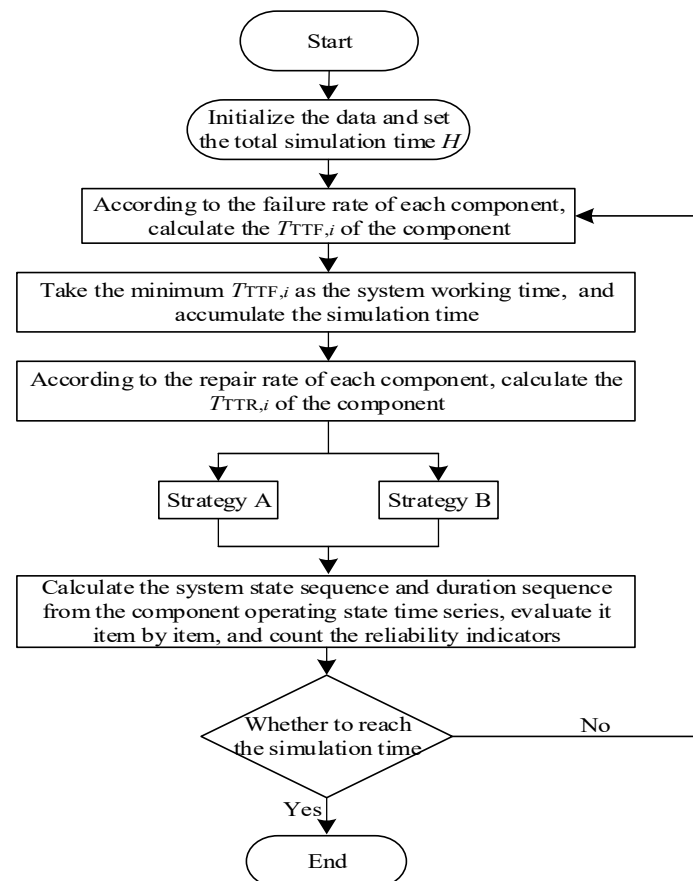


**Figure 4.** Flow chart of the reliability evaluation algorithm under the two strategies.

Step 1. Parameters are initialized.

Step 2. According to the  $\lambda_i$  of each component, Equation (19) is used to randomly sample the  $T_{TTF,i}$  of all components of the microgrid.

Step 3. The minimum  $T_{TTF,i}$  is selected as the normal working time of the system, and simulation time is accumulated.

Step 4. According to the  $\mu_i$  of each component, Equation (20) is used to randomly sample the  $T_{TTR,i}$  of all components of the microgrid.

Step 5. For strategy A and strategy B, shedding of load, the number of power outages, and the outage time are accumulated, respectively.

Step 6. If system simulation time is less than the total simulation time  $H$ , go back to step 2; otherwise, go to the next step.

Step 7. Obtaining the operating state duration sequence of the microgrid system, the load shedding and reliability indicators are calculated, respectively.

#### 4. Case Analysis

For this section, we used the microgrid shown in Figure 1 for reliability analysis; its parameters are shown in Table 1. The research in this paper was completed on a computer configured with an Intel Core i5 processor and 8.0 G memory. The simulation software Matlab R2016a was used to compile the reliability evaluation program of the microgrid system, and the total simulation time  $H$  was set as 87,600 h.

**Table 1.** The reliability parameters of component.

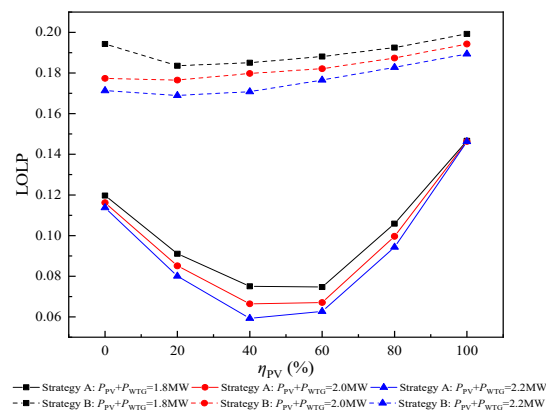
Component	$\lambda_i/(\text{occ}\cdot\text{a}^{-1})$	$\mu_i/(\text{occ}\cdot\text{a}^{-1})$	$\alpha$	$\beta$	$\mu_L$	$\sigma_L$
MT	0.05	0.083	/	/	/	/
WTG	0.05	0.0167	/	/	/	/
PV	0.25	0.0125	2	0.8	/	/
ESS	0.05	0.02	/	/	/	/
Load	/	/	/	/	0	0.1

Just to be clear, the expectation mentioned in the paper is the expectation of load deviation, not the expectation of load. When the expected value of load deviation is 0, it is guaranteed that the probability of load deviation up or down is the same. If the expected value of the load deviation is not 0, or if the expected value of the load deviation is set to positive or negative, then the load deviation may be more biased in the upward or downward direction. In this way, the load fluctuation characteristics cannot be better reflected.

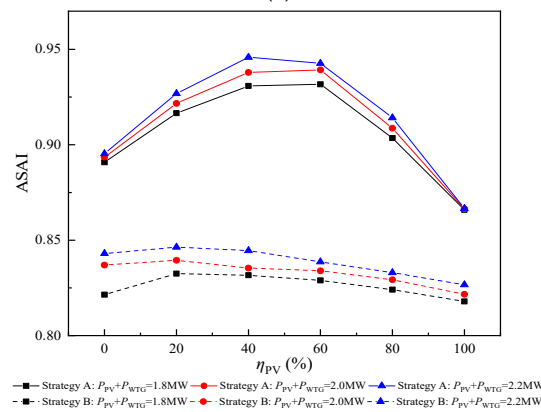
##### 4.1. Analysis of the Influence of WTG and PV Configuration Ratio on System Reliability

In this section, we set the total capacity of WTG and PV to increase from 1.8 MW to 2.2 MW with a step size of 0.2 MW, MT capacity to be 1.6 MW, and ESS capacity and power to be 1 MW·h and 0.3 MW, respectively. Figure 5 depicts the trend of reliability indicators. Among them,  $\eta_{PV}$  represents the proportion of PV in the total capacity of WTG and PV,  $\eta_{PV} = 0\%$  means the system is in the “WTG-ESS” operation state, and  $\eta_{PV} = 100\%$  means the system is in the “PV-ESS” operation state.

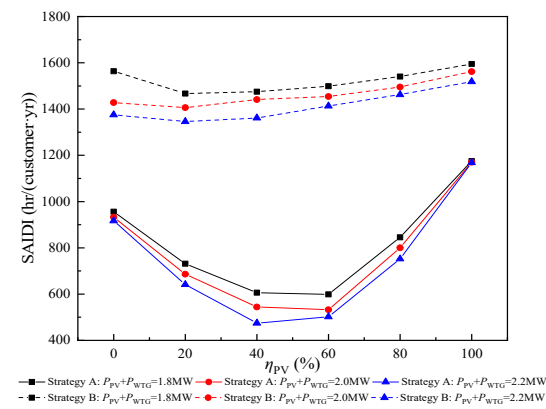
- (1) It can be seen from Figure 5 that when the total capacity of WTG and PV increases from 1.8 MW to 2.2 MW, LOLP, SAIDI, and SAIFI show a decreasing trend while ASAI is the opposite. Therefore, it is useful to increase the total capacity of WTG and PV for reducing the probability, frequency, and duration of system outages and improving the reliability of the microgrid.
- (2) It can also be seen from Figure 5a–d that when the system is in the “PV-WTG-ESS” operating state ( $\eta_{PV}$  varies from 0% to 100%), the reliability indicators are generally better than that of the system in the “WTG-ESS” operating state or in the “PV-ESS” operating state, which is determined by the complementary characteristics of wind and solar. Combined with Figures 2 and 5, it is easier to see the advantages of wind–solar complementary characteristics. In August, the daytime solar intensity is greater and the overall output of PV is greater than that of WTG. When it comes to the night, WTG starts to output and PV is in the output interval. From the perspective of the whole-time scale, the wind–solar complementary characteristics allow the microgrid to receive the energy provided by WTG and PV most of the time. Compared with microgrids containing only PV or WTG, “PV-WTG-ESS” microgrids can better cope with load demand shocks and present a higher reliability.



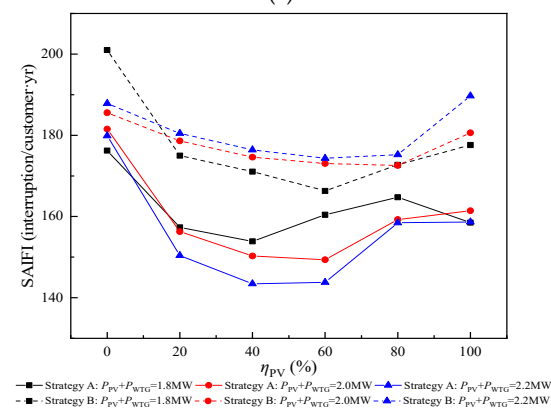
(a)



(b)



(c)



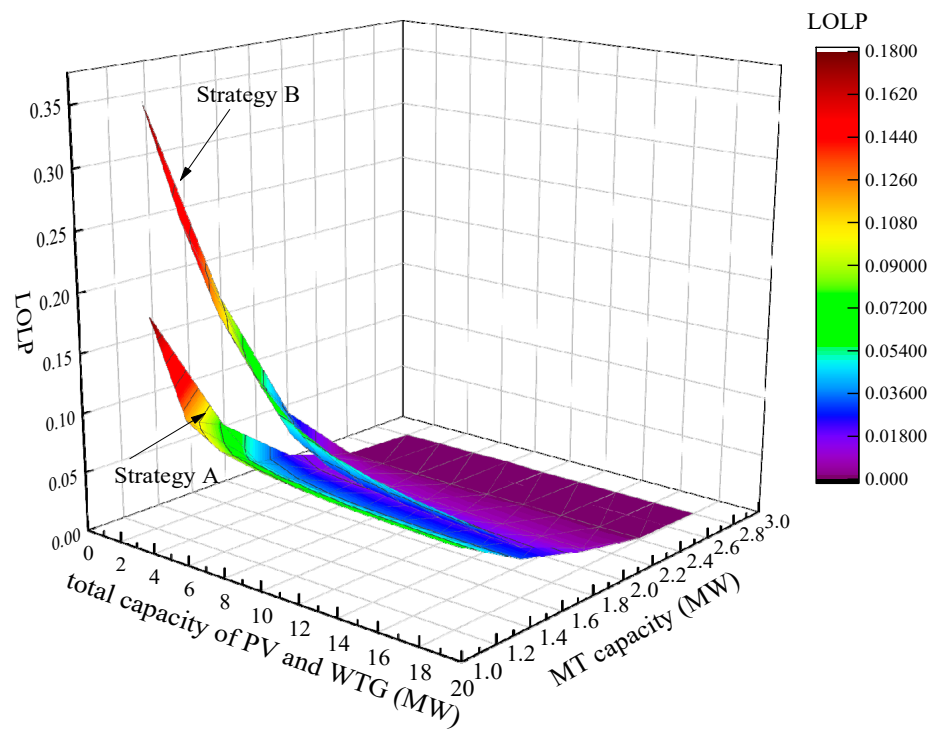
(d)

**Figure 5.** Reliability indicators under different proportions of PV. (a) loss of load probability (LOLP). (b) average service availability index (ASAI). (c) system average interruption duration index (SAIDI). (d) system average interruption frequency index (SAIFI).

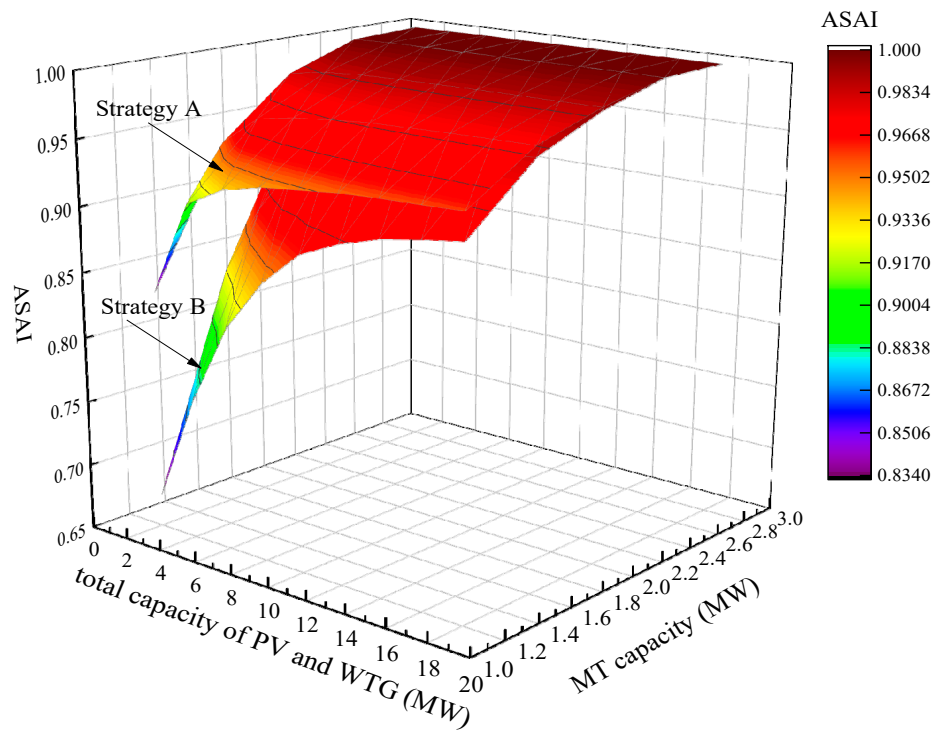
#### 4.2. Analysis of the Influence of WTG, PV, and MT Capacity Changes on System Reliability

In this section, PV and WTG are configured in an equal proportion. The total capacity of WTG and PV increases from 2 MW to 18 MW with a step size of 2 MW, MT capacity increases from 1.2 MW to 2.8 MW with a step size of 0.4 MW, and ESS configuration is consistent with Section 4.1. Figure 6 describes the variation trend of reliability indicators.

- (1) Taking the probability index of LOLP as an example in Figure 6a, when the MT capacity remains unchanged, LOLP will decrease with the increase in the total capacity of PV and WTG and the degree of decrease shows a strong correlation with the total capacity of PV and WTG. Therefore, the range of PV and WTG capacity variation can be divided into the following intervals by the degree of LOLP reduction: 2 MW~6 MW is the completely insufficient capacity interval, 6 MW~12 MW is the capacity insufficient interval, and 12 MW~18 MW is the capacity redundant interval. Obviously, the division of the interval intuitively shows the improvement effect of PV and WTG capacity on probability indicators and provides a basis for PV and WTG capacity configuration. Similarly, this interval division method is also suitable for MT capacity.
- (2) An analysis of the frequency index of SAIFI in Figure 6d showed that, when the MT capacity remains unchanged, the total PV and WTG capacity increases from 2 MW to 18 MW, SAIFI decreases from 305.0543 (interruption/customer·yr) to 211.7951 (interruption/customer·yr), and SAIFI decreases by 30.57%. The reduction is more obvious. However, a further analysis of SAIFI showed that the decrease in SAIFI began to slow down with the increase in PV and WTG total capacity. For example, MT capacity was 1.2 MW. When the total capacity of PV and WTG was increased from 2 MW to 6 MW, the SAIFI was reduced by 17.82%. When the total capacity of PV and WTG was increased from 6 MW to 10 MW, the SAIFI was reduced by 8.45%. When the total capacity of PV and WTG was increased from 10 MW to 14 MW, the SAIFI was reduced by 6.39%. When the total PV and WTG capacity was increased from 14 MW to 18 MW, the SAIFI was reduced by 1.42%. Therefore, increasing the total capacity of PV and WTG is beneficial to rapidly reduce SAIFI. However, when the total capacity of PV and WTG enters the insufficient capacity interval, or even the redundant interval, the output power of PV and WTG can fully meet the load demand, so the SAIFI will maintain a relatively flat state. As for strategy B, SAIFI showed a nonlinear change with the increase in the total capacity of PV and WTG. This is because when the total capacity of PV and WTG is insufficient in the early stage, MT not only supplies power to the residual load but also serves as a renewable energy backup power supply, so the SAIFI is relatively large. When the total capacity of PV and WTG increases to meet the load demand, SAIFI begins to decrease.



(a)



(b)

Figure 6. Cont.

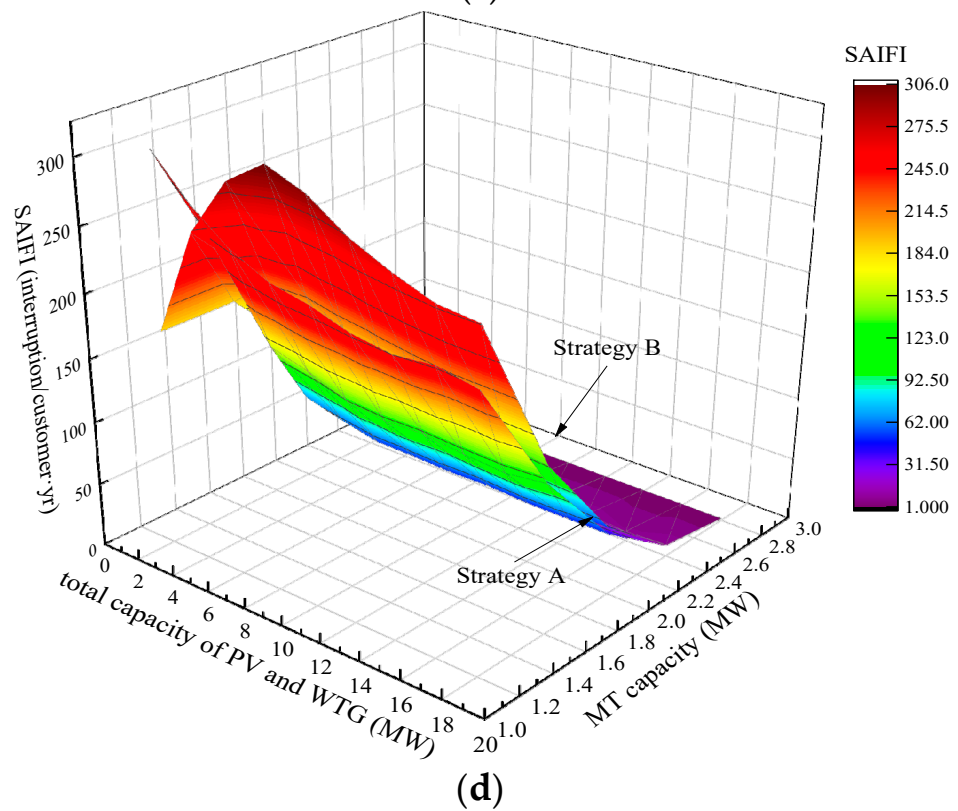
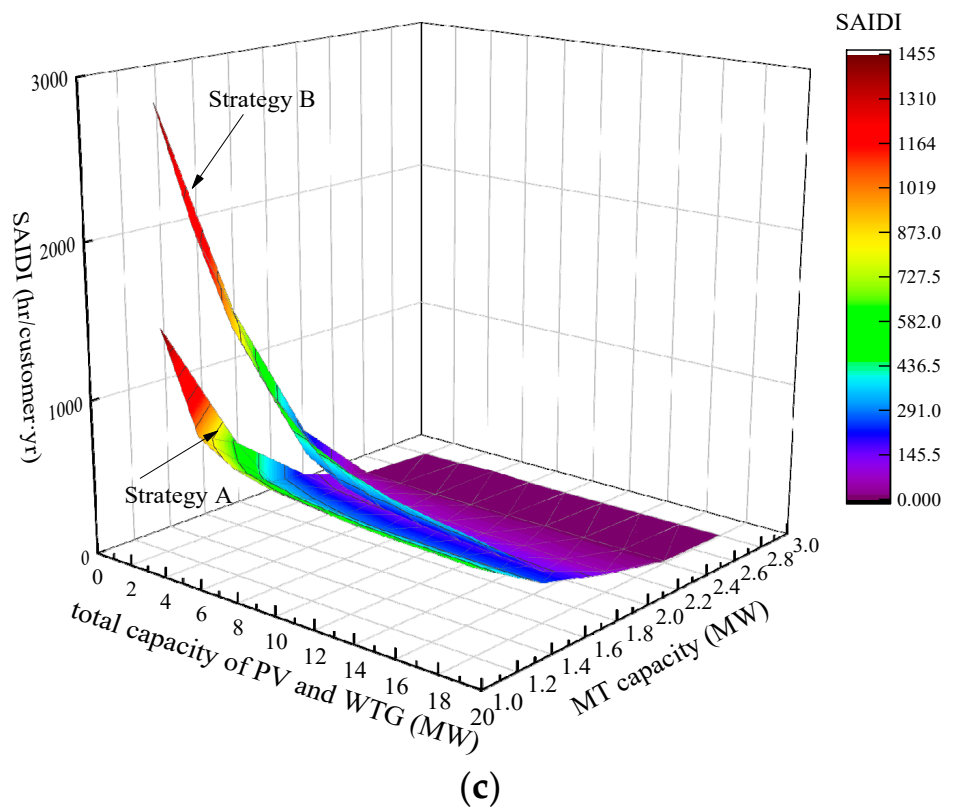


**Figure 6.** Reliability indicators under different capacities of PV, WTG, and microturbine (MT). (a) LOLP. (b) ASAI. (c) SAIDI. (d) SAIFI.

#### 4.3. Analysis of the Influence of PV and WTG Penetration Rate and ESS Capacity Changes on System Reliability

In strategy B, the PV and WTG output can be limited to not exceed 30% of the load demand and the remaining load is supplied by MT and ESS. In order to further analyze the influence of the PV and WTG penetration rate and ESS capacity changes on system reliability, the PV and WTG penetration rate was increased from 30% to 70%, the ESS capacity increased from 1 MW·h to 8 MW·h, and the ESS power was 30% of ESS capacity. Figure 7 describes the variation of reliability indicators.

- (1) Increasing the ESS capacity can improve the reliability in terms of probability, frequency, or duration. It shows that ESS capacity is necessary for the reliable operation of the microgrid. However, the ESS capacity is not “the more, the better”. When the penetration rate of PV and WTG remains at 30%, taking the reliability index ASAI as an example, increasing the ESS capacity can improve ASAI, although the improvement effect gradually becomes slower. When the penetration rate of PV and WTG reaches 70%, with the increase in ESS capacity, the effect of ESS on reliability improvement gradually becomes weaker. This phenomenon shows that, with the increase in PV and WTG permeability, the capacity of ESS to improve ASAI becomes smaller and smaller. Due to the stochastic performance of PV and WTG, the larger the proportion of power supply that PV and WTG are responsible for, the higher the probability is of a mismatching load demand. More ESS capacity is used to maintain the balance between them, which results in very limited remaining ESS capacity for improving reliability; so, the effect of ESS on reliability improvement tends to be saturated.
- (2) When the PV and WTG penetration rates gradually increase, the output uncertainty of PV and WTG will increase and affect the reliability of the microgrid. At this time, ESS can play an important role in the smoothing effect.
- (3) Comparing strategy A and strategy B, it can be seen that strategy A adopts the principle of priority output and consumption of PV and WTG and maximum output of MT and ESS, which reduces the number and frequency of load shedding, so that the load demand can be a maximized degree of satisfaction. In strategy B, the ESS is only responsible for the output of PV and WTG to maintain a certain proportion of load supply (that is, the ESS is used to achieve the controllability of PV and WTG output) and does not participate in the power supply in other scenarios. For example, PV, WTG, and ESS are only responsible for supplying power to a part of the load. When the output of the MT cannot meet the demand of the remaining load, only load reduction can be performed, even if the ESS still has remaining capacity. This can result in load demands not being fully met, which risks reducing reliability. Compared with strategy A, the ESS function in strategy B has not been fully utilized and the number of load reductions is relatively large. It was shown that strategy B achieves controllability of PV and WTG at the expense of reliability, which is a good explanation for the reliability level of the microgrid with strategy B as lower than that with strategy A.

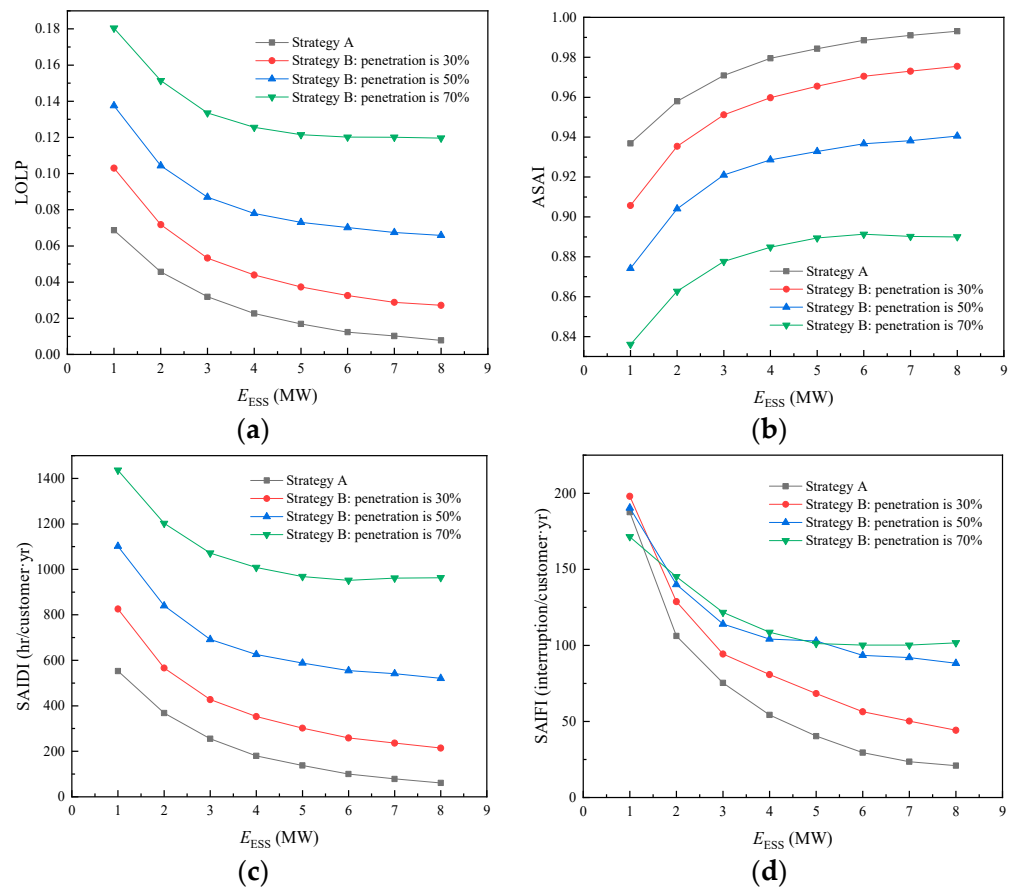


**Figure 7.** Reliability indicators under different penetration rates of PV and WTG and capacity of ESS. (a) LOLP. (b) ASAI. (c) SAIDI. (d) SAIFI.

## 5. Conclusions

In this work, a microgrid system including WTG, PV, MT, ESS, and loads was established, a reliability evaluation framework was established, two different load shedding strategies were formulated, and simulation analysis was carried out in the test system. The main conclusions of this paper are as follows:

- (1) When WTG and PV are both connected to the microgrid, the complementary characteristics of wind and solar can significantly improve the reliability of the microgrid, which is better than the microgrid system that only contains PV or WTG.
- (2) Increasing the total capacity of PV and WTG can improve the reliability of the microgrid, and the total capacity of PV and WTG can be reasonably planned according to the improvement effect. In addition, the use of PV, WTG, and MT to cooperate with each other is also a good choice for improving reliability.
- (3) The increase in the penetration rate of renewable energy has exacerbated the uncertainty of the power supply, which has impacted the reliability of the microgrid. For this reason, more ESS is required to meet the load demand.
- (4) Comparing strategy A and strategy B, we found that strategy A focuses on ensuring that the microgrid supplies power to the load and minimizes the number and probability of reduction. Strategy B focuses on improving the controllability of PV and WTG output power at the expense of microgrid reliability. It shows that strategy A has more advantages in improving the reliability of the microgrid.

The distributed energy, ESS, load, and other elements in the microgrid present polymorphic uncertainty in terms of operation mechanism and output characteristics, for example, the “failure–repair” time series life characteristics of components, the randomness and fluctuation of PV and WTG output, the probability distribution of wind speed, the time

varying and randomness of load, the power characteristics of ESS, and inherent characteristics such as equipment age. In addition, with the development of microgrids, the flexible access of distributed energy resources and changes in equipment capacity are inevitable such as the increase or decrease in ESS capacity on the supply side and the increase in the load of power users on the demand side. These issues will bring great challenges to the reliability operation and reliability evaluation of microgrids. Therefore, establishing a perfect probabilistic simulation model of polymorphic uncertainty in a microgrid is the basis for reliability assessment and capacity planning. The uncertainty characteristics of a microgrid are very complex. In the future, we will focus on multi-state uncertainty modeling and mechanism analysis of a microgrid, and then support the reliability assessment and system planning of a microgrid.

**Author Contributions:** Conceptualization, Z.W. and J.Z.; methodology, Z.W. and J.Z.; software, Z.W.; validation, Z.W., J.Z. and Z.Z.; formal analysis, Z.W.; investigation, Z.W. and J.Z.; resources, Z.Z.; data curation, Z.W.; writing—original draft preparation, Z.W. and J.Z.; writing—review and editing, Z.W. and Z.Z.; visualization, Z.W.; supervision, Z.W. and J.Z.; project administration, J.Z.; funding acquisition, J.Z. All authors have read and agreed to the published version of the manuscript.

**Funding:** This paper was supported by the National Key R&D Program of China (No. 2021YFE0103800) and Beijing High Level Innovation Team Construction Plan (No. IDHT20180502).

**Institutional Review Board Statement:** Not applicable.

**Informed Consent Statement:** Not applicable.

**Data Availability Statement:** Not applicable.

**Conflicts of Interest:** The authors declare no conflict of interest.

## Nomenclature

Symbol	Meaning of Each Symbol
$P_L(h)$	Total load power
$P_{MT}(h)$	MT power output
$P_{PV}(h)$	Power output
$P_{WTG}(h)$	WTG power output
$P_{ESS}(h)$	ESS power output
$P_{MT}^{max}(h)$	MT maximum power output at $h$ -th moment
$T_{TTF,i}^{MT}$	Fault free working state sequence of the MT
$T_{TTF,i}^{MT}$	Faulty working state sequence of the MT
$F_{MT}(h)$	Working state function of MT
$P_{WTG}^{max}(h)$	Maximum power output per hour of the WTG
$F_{WTG}(h)$	Working state function of WTG
$P_r$	WTG rated power output
$V$	Wind speed
$V_{ci}$	Cut-in wind speed
$V_r$	Rated wind speed
$V_{co}$	Cut-out wind speed
$T_{TTF,i}^{WTG}$	Fault free working state sequence of the WTG
$T_{TTR,i}^{WTG}$	Faulty working state sequence of the WTG
$P_{PV}^{avail}(h)$	PV power output during the illumination period
$f(P_{PV}^{avail}(h))$	Distribution function of the $P_{PV}^{avail}(h)$
$T_{sun}^{rise}$	Sunrise time
$T_{sun}^{down}$	Sunset time
$\Gamma$	Gamma function
$\alpha$	Shape parameter of the beta distribution
$\beta$	Shape parameter of the beta distribution
$F_{PV}(h)$	Working state function of PV
$T_{TTF,i}^{PV}$	Fault free working state sequence of the PV

$T_{TTR,i}^{PV}$	Faulty working state sequence of the PV
$S_{SOC}(h)$	SOC of ESS at the $h$ -th moment
$\delta$	ESS self-discharging rate
$P_{ch}(h)$	Charging power
$P_{dch}(h)$	Discharging power
$\eta_{ch}$	ESS charging efficiency
$\eta_{dch}$	ESS discharging efficiency
$\Delta t$	Simulation step
$E_{ESS}^{max}$	Upper limit of ESS capacity
$F_{ch}(h)$	State function of charging
$F_{dch}(h)$	State function of discharging
$S_{SOC}^{max}$	Upper limit of the SOC
$S_{SOC}^{min}$	Lower limit of the SOC
$P_L^T(h)$	Hourly time-varying component of load
$P_L^R(h)$	Randomness component of load
$P_y$	Annual peak load
$P_{y-m}$	Percentage of the monthly peak load to the annual peak load
$P_{m-d}$	Percentage of the daily peak load to the monthly peak load
$f(P_L^R(h))$	Density function of load randomness
$P_{d-h}$	Percentage of hourly peak load to the daily load
$\mu_L$	Expectation deviation of $f(P_L^R(h))$
$\sigma_L$	Standard deviation of $f(P_L^R(h))$
$T_{TTF,i}$	Fault free working state sequence
$\lambda_i$	Failure rate of component $i$
$\mu_i$	Repair rate of component $i$
$T_{TTR,i}$	Faulty working state sequence
$u_i, \zeta_i$	Random variable of the uniform distributions
$R_{LOLP}$	Reliability indicator of LOLP
$H$	Total simulation time
$F_{LOLP}(h)$	State function of LOLP
<b>Symbol</b>	<b>Meaning of Each Symbol</b>
$R_{ASAI}$	Reliability indicator of ASAI
$R_{SAIDI}$	Reliability indicator of SAIDI
$R_{SAIFI}$	Reliability indicator of SAIFI
$U_i$	The annual outage time of users of $i$ -th load point
$N_i$	Number of users of $i$ -th load point
$N_{LP}$	Total number of load points
$\lambda_i$	The annual power failure frequency of $i$ -th load point

## References

- Guo, X.S.; Lou, S.H.; Wu, Y.W.; Wang, Y.C. Low-Carbon Operation of Combined Heat and Power Integrated Plants Based on Solar-Assisted Carbon Capture. *J. Mod. Power Syst. Clean Energy* **2022**, *in press*.
- Muhammad, H.S.; Wang, F.Z.; Basheer, A.K.; Sajid, I. A Review on Microgrids' Challenges & Perspectives. *IEEE Access* **2021**, *9*, 166502–166517.
- Wang, Y.; Xie, K.G.; Hu, B.; Wang, L.Y. Reliability Analysis of Islanded Microgrid Based on Sequential Simulation. *Trans. China Electrotech. Soc.* **2016**, *31*, 206–211.
- Zhou, B.R.; Huang, T.C.; Zhang, Y.J. Reliability Analysis on Microgrid Considering Incentive Demand Response. *Autom. Electr. Power Syst.* **2017**, *41*, 70–78.
- Wang, Y.; Wan, L.Y.; Hu, B.; Xie, K.G.; Xiang, B. Isolated Island Operating Characteristics Based Analysis on Reliability of Microgrid. *Power Syst. Technol.* **2014**, *38*, 2379–2385.
- Bahramirad, S.; Reder, W.; Khodaei, A. Reliability-Constrained Optimal Sizing of Energy Storage System in a Microgrid. *IEEE Trans. Smart Grid* **2012**, *3*, 2056–2062. [[CrossRef](#)]
- Song, X.T.; Zhao, Y.X.; Zhou, J.H.; Weng, Z.P. Reliability varying characteristics of PV-ESS-Based standalone microgrid. *IEEE Access* **2019**, *7*, 120872–120883. [[CrossRef](#)]
- Guo, L.; Yu, Z.Z.; Wang, C.S.; Li, F.X.; Schiettekatte, J.; Deslauriers, J.-C.; Bai, L.Q. Optimal Design of Battery Energy Storage System for a Wind—Diesel off-grid Power System in a Remote Canadian Community. *IET Gener. Transm. Distrib.* **2016**, *10*, 608–616. [[CrossRef](#)]

9. Wang, S.X.; Zhang, X.Y.; Ge, L.J.; Wu, L. 2-D Wind Speed Statistical Model for Reliability Assessment of Microgrid. *IEEE Trans. Sustain. Energy* **2016**, *7*, 1159–1169.
10. Hadis, M.; Mahdi, E.; Amir, A.; Ali, Z. Modeling a Hybrid Microgrid Using Probabilistic Reconfiguration under System Uncertainties. *Energies* **2017**, *10*, 1430. [[CrossRef](#)]
11. Azeem, F.; Narejo, G.B.; Shah, U.A. Integration of Renewable Distributed Generation with Storage and Demand Side Load Management in Rural Islanded Microgrid. *Energy Effic.* **2020**, *13*, 217–235. [[CrossRef](#)]
12. Al-Muhaini, M.; Heydt, G.T. Evaluating Future Power Distribution System Reliability Including Distributed Generation. *IEEE Trans. Power Deliv.* **2013**, *28*, 2264–2272. [[CrossRef](#)]
13. Gao, Y.J.; Zhu, J.; Cheng, H.X.; Liang, H.F.; Li, P. Evaluation on the Short-term Power Supply Capacity of Active Distribution System Based on Multiple Scenarios Considering Uncertainties. *Proc. CSEE* **2016**, *36*, 6076–6085.
14. Zhao, Y.; Wang, J.; Geng, L.; Wang, Y.P.; Shuang, Y.J. An Extended Cross Entropy Method for Non-sequential Monte Carlo Simulation of Power System Reliability Assessment. *Proc. CSEE* **2017**, *37*, 1963–1974.
15. Ding, Y.; Singh, C.; Goel, L.; Ostergagrd, J.; Wang, P. Short-Term and Medium-Term Reliability Evaluation for Power Systems with High Penetration of Wind Power. *IEEE Trans. Sustain. Energy* **2014**, *5*, 896–906. [[CrossRef](#)]
16. Fu, Q.; FMontoya, L.; Solanki, A.; Nasiri, A.; Bhavaraju, V.; Abdallah, T.; CYu, D. Microgrid Generation Capacity Design with Renewables and Energy Storage Addressing Power Quality and Surety. *IEEE Trans. Smart Grid* **2019**, *3*, 2019–2027. [[CrossRef](#)]
17. Wang, C.S.; Zhang, T.Y.; Luo, F.Z.; Li, F.X.; Liu, Y.Z. Impacts of cyber system on microgrid operational reliability. *IEEE Trans. Smart Grid* **2019**, *10*, 105–115. [[CrossRef](#)]
18. *IEEE Std1366–2003*; IEEE Guide for Electric Power Distribution Reliability Indices—Redline. IEEE: New York, NY, USA, 2012; pp. 1–92.